termis.

Tissue Engineering
& Regenerative Medicine
International Society

Open camera or QR reader and
scan code to access this article
and other resources online.

## ORIGINAL ARTICLE

# A Multilayer Nanofibrous Mat for the Topical Chemotherapy of the Positive Margin in Bladder Cancer

Jing Wang, PhD,[1] Minglong Wu, PhD,[2] Yunpeng Zhu, PhD,[3] Zhixian Wang, MD,[1] Heng Cao, MS,[4] Xing Li, MS,[1] Yisheng Yin, MS,[1] Xiang Ren, MS,[1] Yiqun Tian, MS,[1] Zihao Guo, MS,[1] and Xiaoyong Zeng, MD, PhD[1]

Treatment of positive margins after solid tumor resection remains a significant challenge for clinicians. Owing to unique structural features, electrospun nanofibrous mats are promised to be an implantable antitumor system
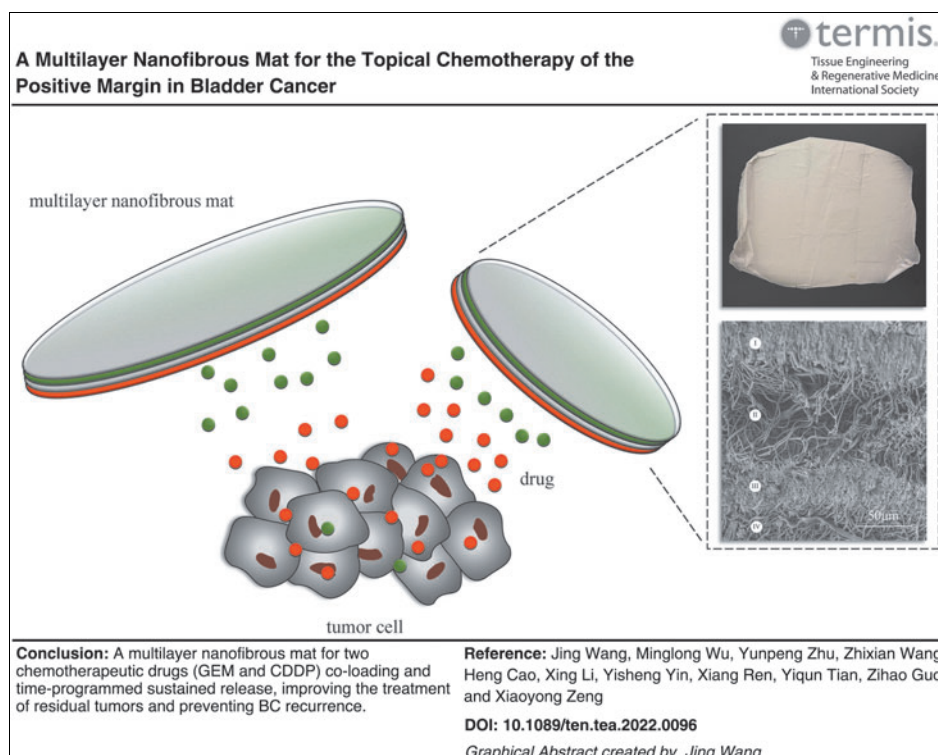
(*Color images are available online*).

Departments of [1]Urology, [2]Surgery, [3]Thoracic Surgery, and [4]Gynaecology and Obstetrics, Tongji Hospital, Tongji Medical College, Huazhong University of Science and Technology, Wuhan, China.

through the delivery of active agents in a controlled manner. In this study, we utilized sequential electrospinning to fabricate a multilayer mat in which gemcitabine (GEM) and cisplatin (CDDP) were electrospun individually in distinct layers. By designing the structure, the multilayer mat could deliver antitumor agents sustainedly and prolong the release of GEM, which is loaded in the inner layer. *In vitro* assays show that the multilayer mats effectively inhibit bladder cancer (BC) cells and elevate apoptosis. In animal models of BC, the implantable drug-loaded fibrous mat can effectively treat positive margins and prevent local recurrence. Moreover, the local delivery of GEM and CDDP significantly lowers liver toxicity compared with systemic chemotherapy. In summary, a multilayer nanofibrous mat is developed for the localized and controlled delivery of GEM, dramatically improving the treatment of residual tumors and preventing BC recurrence.

**Keywords:** electrostatic spinning, drug delivery system, topical chemotherapy, bladder cancer, positive surgical margin

## Impact Statement

The designed multilayer nanofibrous mats can achieve two chemotherapeutic drugs (gemcitabine and cisplatin) co-loading and time-programmed sustained release, significantly improving our previous study. The antitumor effect of the drug-loaded mat *in vivo* and *in vitro* was sufficiently demonstrated. We expect to bring a new strategy of topical chemotherapy for treating positive surgical margins in bladder cancer.

## Introduction

URINARY BLADDER CANCER (BC) is one of the most common malignancies worldwide, with about 573,000 new cases and 213,000 deaths in 2020.[1] Radical cystectomy (RC) with bilateral pelvic lymph node dissection is the standard therapy for localized muscle-invasive tumors.[2] Surgical margin status is not only related to the risk of local recurrence but is also associated with disease progression and disease-specific mortality.[3,4] Therefore, surgical resection is usually followed by adjuvant chemotherapy. Adjuvant chemotherapy eliminates potential residual malignant cells, and localized implants as drug delivery systems show significant potential for BC treatment.[5]

Drug-loaded electrospun fiber mats were reported as promising candidates with remarkable properties, such as high drug capacity, specific surface area, and ease in preparation and handling.[6–8] It was demonstrated to expand local drug concentration and decline toxic side effects effectively.[9,10] Many antitumor drugs, such as paclitaxel, 5-fluorouracil, daunorubicin, and hydroxycamptothecin, have been electrospun into nanofibers.[11–14] Gemcitabine (GEM), in combination with cisplatin (CDDP), is the most commonly used standard first-line treatment for urothelial carcinoma. Recent international guidelines suggest CDDP-based neoadjuvant chemotherapy followed by RC for patients with muscle-invasive BC, and GC adjuvant chemotherapy is also an option for select patients.[2,15]

Our earlier study utilized electrospinning to prepare a drug-loaded sustained-release mat.[16] The chemotherapy drugs, GEM and CDDP, were mixed and electrospun in a monolayer fiber mat and released simultaneously, which is inconsistent with the administration sequence of the GC regimen for BC chemotherapy in clinical practice. However, individual drug release orders should be controlled in combination systems.[17] Previous articles reported multilayer electrospun mats for sustained single drug release.[18]

Herein, in this study, a new drug delivery carrier was prepared by sequential electrospinning. The designed mats can achieve two chemotherapeutic drugs (GEM and CDDP) co-loading and time-programmed sustained release. We adequately verified improved antitumor activity and reliable toxicity of the drug-loaded mats *in vivo* and vitro. Our study would accelerate the clinical application of composite multilayer drug-loaded fiber mats.

## Materials and Methods

### Materials

Poly(lactic acid) (PLA, Mw = 100,000) was obtained from Guanghua Co. Ltd. *N,N*-Dimethylformamide (DMF) and 1,1,1,3,3,3-hexafluoro-2-propanol (HFIP) were purchased from Aladdin, Inc. GEM was purchased from Hubei Yibantian Pharmaceutical Co. Ltd. CDDP was purchased from Qilu Pharmaceutical Co. Ltd.

### Preparation of drug-loaded multilayer nanofibrous mats

GEM/CDDP-loaded multilayer nanofibrous mat (multi-GC@PLA mat) was fabricated using sequential electrospinning. In brief, the basal layer (PLA layer) was prepared by electrospinning of PLA/HFIP (20% w/v) electrospun liquid. The GEM-loaded mat (G@PLA layer) was prepared by electrospinning of PLA and GEM mixture (GEM/PLA, 10% w/w) in HFIP. The barrier layer (PLA layer) was prepared by electrospinning of the PLA/HFIP solution (20% w/v) following the G@PLA layer. The CDDP-loaded layer (C@PLA layer) was prepared by electrospinning of the solution of PLA and CDDP (CDDP/PLA, 5% w/w) in HFIP/DMF (90/10, v/v) at a polymer concentration of 20% w/v (Fig. 1). The electrospinning parameters were set as follows: 15 kV; 0.16 mm/min; 18 cm. All the experiments were prepared at room temperature.

The rhodamine B and indocyanine green-loaded multilayer nanofibrous mat (multi-RI@PLA mat) were prepared as described earlier (Supplementary Fig. S1). GEM/CDDP-loaded monolayer nanofibrous mat (mono-GC@PLA mat) and PLA nanofibrous mat were identically prepared as a control.
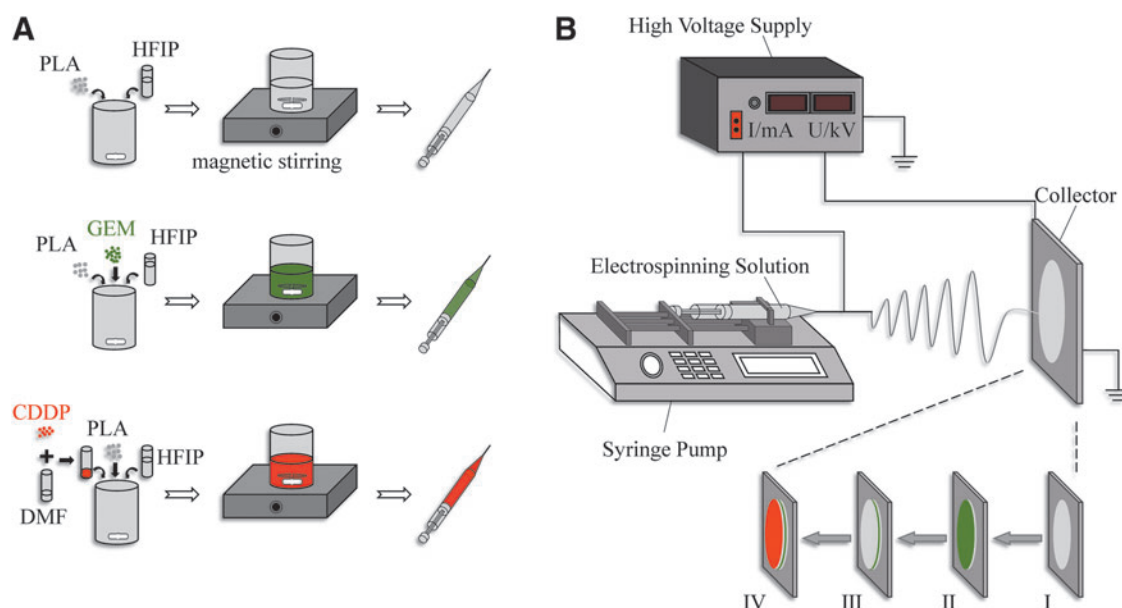
**FIG. 1.** Schematic illustration of the fabrication process of the sequential electrospinning. **(A)** Electrospinning solution preparation process. **(B)** Electrostatic spinning process. The multilayered nanofibrous mat (multi-GC@PLA mat) was fabricated in the following order: (I) the basal layer (PLA layer), (II) the GEM-loaded layer (G@PLA layer), (III) the barrier layer (PLA layer), and (IV) the CDDP-loaded layer (C@PLA layer). PLA, poly(lactic acid); DMF, *N,N*-dimethylformamide; HFIP, 1,1,1,3,3,3-hexafluoro-2-propanol; GEM, gemcitabine; CDDP, cisplatin. Color images are available online.

### Morphological analysis

The surface and section of the mats were scanned by scanning electron microscope (SEM). The distribution of fiber diameters was analyzed using ImageJ software.

### In vitro *drug release study*

In brief, dry samples (multi-GC@PLA mat and mono-GC@PLA mat) were weighed and placed in the dark beaker, and 100 mL of 0.9% normal saline with 1% Tween 80 was used as the solvent. The beaker was placed in the incubator (37°C). One milliliter eluent was collected at various time points (0.5, 1, 2, 4, 8, 12, 18, 24, and 48 h), and an equal volume solvent was added to keep the total volume of 100 mL. High-performance liquid chromatography (HPLC) was used to measure the concentrations of the GEM. For HPLC, a $C_{18}$ column ($4.6 \times 15$ cm, 5 mm) and the mobile phase (0.05 M ammonium acetate buffer, pH 5.7, methanol, 90/10, v/v) were used (Supplementary Fig. S2).

To calculate the mat's load drug rate, a certain mass of the multi-GC@PLA mat was weighed and dissolved in chloroform ($CHCl_3$) and then transferred to ultrapure water by extraction. The HPLC measured the GEM concentration in ultrapure water. The load drug rate was recorded as the ratio of the measured value to the theoretical value of GEM.

### In vitro *antitumor efficacy*

Murine BC cell line, MB49, was obtained from Guangzhou Jinio Biotechnology Co. Ltd. and cultured in RPMI-1640 medium (RPMI-1640; Gibco) with 10% fetal bovine serum (FBS; Gibco) at (37°C, 5% $CO_2$).

The MB49 cells were divided into five groups. The MB49 cells in the control group were treated with phosphate-buffered saline (PBS; Gibco). The MB49 cells in the PLA group, the mono-GC@PLA group, and the multi-GC@PLA group were treated with one round slice of the PLA mat, mono-GC@PLA mat, and the multi-GC@PLA mat, respectively. The MB49 cells in the drug group were treated with 0.4 μg/mL GEM and 0.2 μg/mL CDDP (the approximate amount of drug loaded on one piece of the mat). The cells in five groups were collected at 6, 12, and 24 h, respectively. The apoptotic cell rate was detected by the Annexin-FITC/PI Apoptosis Kit (Annexin-FITC/PI; BD). The expression of Caspase3 among the five groups was tested by western blotting (Antibody of Caspase3; CST).

### Biodistribution study

For visualization of drug release from multilayer nanofibrous mats, the multi-RI@PLA mat was implanted under the groin of health C57BL/6 mice. The mice were imaged

**FIG. 2.** Properties of the multilayered nanofibrous mats. Representative images of **(A)** the multi-GC@PLA mat. The multi-GC@PLA mat was cut into the **(B)** round patch, with a diameter of about 5 mm. **(C)** GEM release from the mono-GC@PLA mat and the multi-GC@PLA mat in 0.9% normal saline with 1% Tween 80. **(D)** The sectional SEM image revealed the four consecutive layered structures. SEM images of the surface of **(E)** multi-GC@PLA mat and **(F)** PLA mat and the histograms showed fiber diameter distribution. Color images are available online.
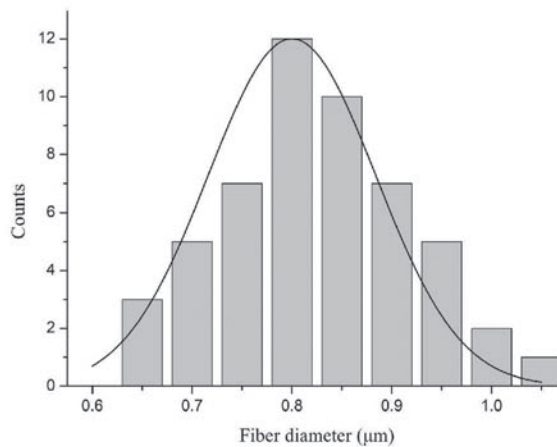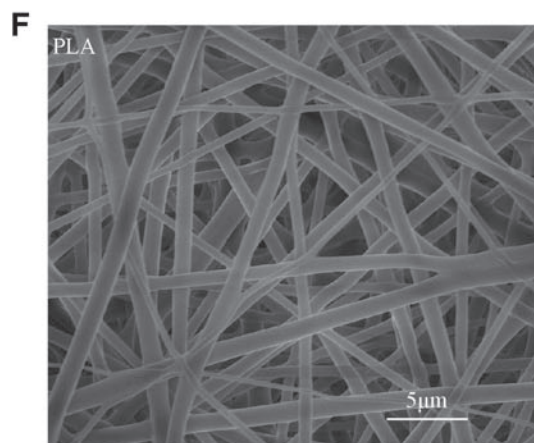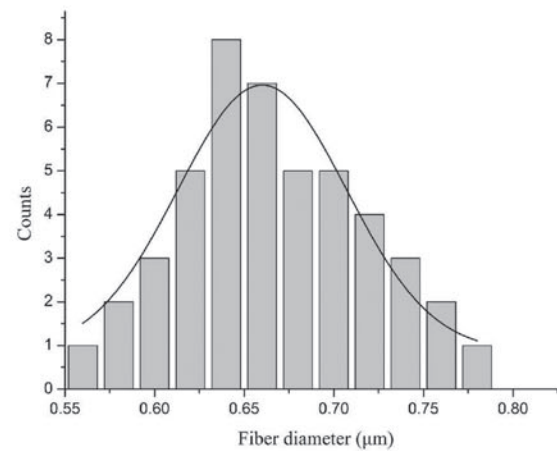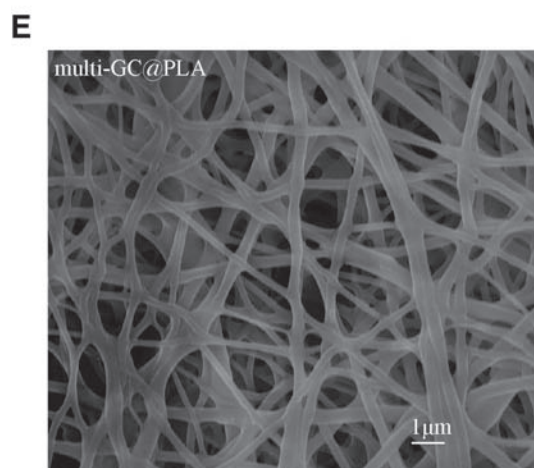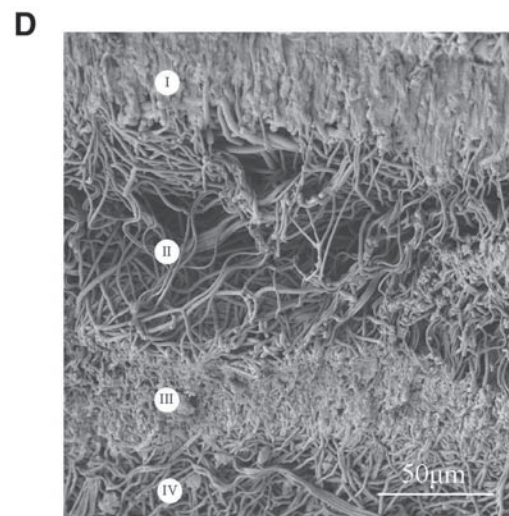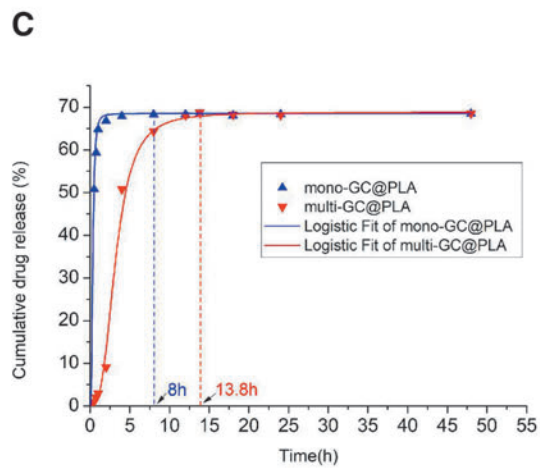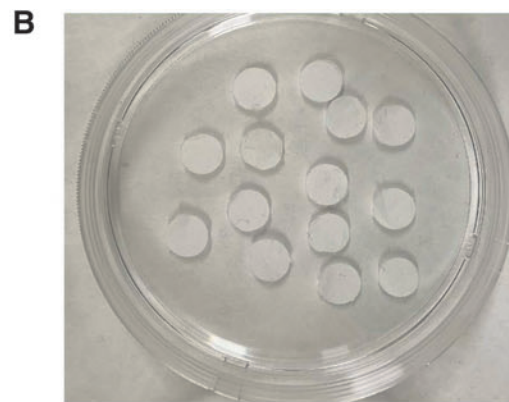
by a fluorescent imaging system (IVIS SPECTRUM system; Caliper Life Science) to detect the distribution of rhodamine B and indocyanine green.

The ultra-performance liquid chromatography-triple quadrupole tandem mass spectrometry (UHPLC-MS/MS; Agilent Technologies) was used to detect drug accumulation and distribution of the GEM in the liver, kidney, blood, and tumor tissue. On the 21st day after the operation, liver, kidney, tumor, and blood samples were collected. For the tissue sample, a certain tissue mass was weighed and fully ground in the extraction solution (methanol:water = 3:1), and the supernatant was collected by centrifugation for UHPLC-MS/MS. An adequate amount of serum was mixed with methanol for the blood sample, and the supernatant was collected by centrifugation for UHPLC-MS/MS.

*In vivo* antitumor efficacy evaluation. A positive surgical margin model was established in C57BL/6 mice (male, 6–8 weeks old). Primary subcutaneous tumors were induced by injection of the MB49 cells ($2.5 \times 10^7$ in 0.5 mL PBS) in the left groin of mice. After the tumor grew to $100 \, mm^3$, the mice were anesthetized (1% pentobarbital, 0.05 mL/10 g body weight, i.p) and exposed to the tumor. A portion of the tumor was removed to establish a positive surgical margin.[16]

Mice were randomized to five groups ($n = 12$), including the control group, the PLA group, the mono-GC@PLA group, the multi-GC@PLA group, and the drug group. Mice underwent resection only in the control group. In the mono-GC@PLA group or the multi-GC@PLA group, two round slices of drug-loaded mats were directly pasted on the resection site. For comparison, mice were implanted with the PLA mats at the incision edge of the tumor. Mice in the drug group were injected intraperitoneally with CDDP (0.02 mg/10 g) + GEM (0.04 mg/10 g) once a week.

Tumor volume was measured and recorded. On the 21st day after the operation, the tumors were extracted and weighed and sections for further histological analysis (H&E and TUNEL).

Three mice were selected randomly from each group for safety evaluation on the 7th, 14th, and 21st days after the operation. The blood plasm samples were collected for measuring clinic parameters, including aspartate aminotransferase (AST), alanine aminotransferase (ALT), creatinine (CR), and blood urea nitrogen (BUN).

The animal study was supervised by the Ethics Committee of Tongji Medical College and performed according to the National Institutes of Health Guidelines for the Care and Use of Laboratory Animals.

### Statistical analysis

All data are presented as mean ± standard deviation (SD) and analyzed using SPSS software (Version 23.0; SPSS). Differences in mean values were tested by the independent sample *t*-test for two groups. Statistical significance was accepted with a *p*-value <0.05.

## Results

### Properties of nanofibers and mats

In general, the surface of the fiber mat is smooth, with a uniform thickness (Fig. 2A, B). In the multi-GC@PLA mat,

the sectional SEM image revealed four consecutive layered structures (Fig. 2D). The fibers in the drug-loaded mat were staggered into the network structure, with smooth surface, and no obvious beading defects. The quantitative analysis showed that the average diameter of fibers in the multi-GC@PLA mat and the PLA mat was 664.41 ± 80.25 nm and 824.88 ± 93.12 nm, respectively (Fig. 2E, F).

The load drug rate was about 93.8% ± 0.2%. The drug-releasing curve (the mono-GC@PLA mat and the multi-GC@PLA mat) is shown in Figure 2C. The cumulative GEM release of the mono-GC@PLA mats increased rapidly during the initial 1-h period, followed by a slow and sustained release, ending with the dissolution equilibrium. The dissolution equilibrium of the mono-GC@PLA mat was reached at 8 h. Compared with the mono-GC@PLA, the cumulative release percentage of GEM in the multi-GC@PLA mat was <10% in the first 4 h, and the time to reach maximum release was delayed by 5.8 h.

### In vitro *antitumor efficacy*

As shown in Figure 3A, there was no significant change in the apoptosis rate in the Con group and the PLA group during the observation period, and the difference in the rate between the two groups was not statistically significant (6 h, $p = 0.5068$; 12 h, $p = 0.6956$; 24 h, $p = 0.7824$). The apoptotic cells in the mono-GC@PLA group, the multi-GC@PLA group, and the drug group significantly increased during the 24 h. At 6 and 12 h, the rate of apoptotic cells in the drug group was significantly higher than that of the multi-GC@PLA group (6 h, $p < 0.0006$; 12 h, $p = 0.0015$). After the treatment with the drug-loaded mats for 24 h, the percentage of apoptotic cells in the multi-GC@PLA group was higher (85.27 ± 1.38 vs. 73.53 ± 2.36, $p = 0.0128$).

Similar to the flow cytometry results, there was no significant change in the expression of Caspase3 in the Con group and the PLA group, and the difference between the two groups was not statistically significant (6 h, $p = 0.9483$; 12 h, $p = 0.5570$; 24 h, $p = 0.8716$). The Caspase3 expression in the drug group was significantly lower than that of the multi-GC@PLA group (6 h, $p = 0.0056$; 12 h, $p = 0.0278$).

### Biodistribution study

Biodistribution studies suggested that the released rhodamine B and indocyanine green are mainly concentrated in the tissue underneath the implanted mats. The trend of fluorescence intensity of the two dyes was similar, decreasing rapidly during the initial period, followed by a slight and sustained decrease until the fluorescence signal completely disappeared (Fig. 4A).

Accumulation and distribution of the GEM in the liver, kidney, blood, or tumor tissue were detected by the UHPLC-MS/MS. Compared with the drug group, mice in the multi-GC@PLA group had lower levels of GEM in the livers (1509.97 ± 76.42 vs. 813.48 ± 60.71, pg/g; $p < 0.001$), kidneys (502.39 ± 35.41 vs. 235.52 ± 34.93, pg/g; $p = 0.001$) and blood (1729.06 ± 56.33 vs. 1208.02 ± 38.73, pM; $p < 0.001$), conversely, higher levels in tumor tissue (832.93 ± 49.14 vs. 6993.01 ± 137.08, pg/g; $p < 0.001$) (Fig. 4B).
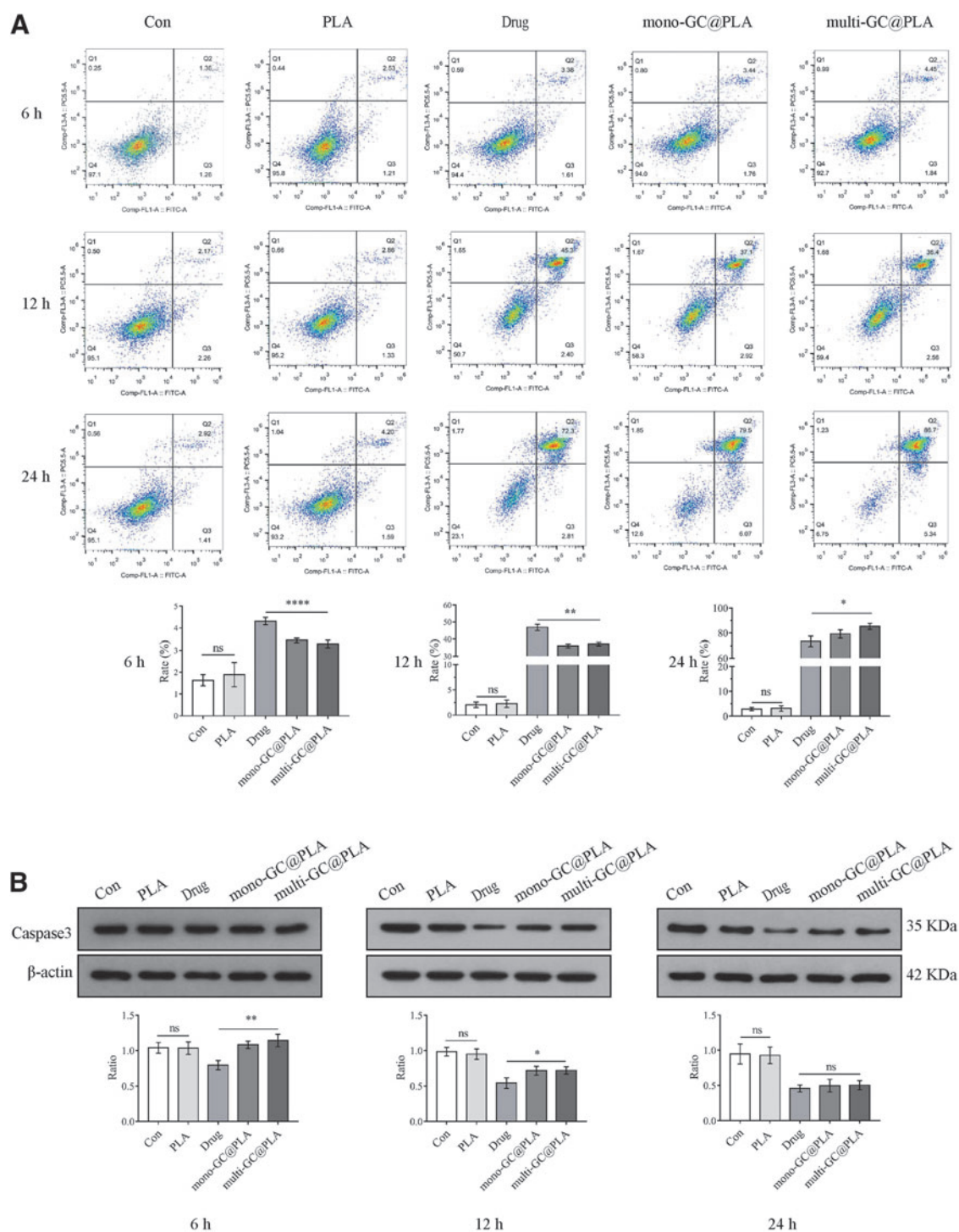
**FIG. 3.** Study of the antitumor efficacy *in vitro*. **(A)** The apoptotic cell percentage was measured by flow cytometry, and **(B)** the western blotting presented the expression of Caspase3 of the MB49 cell in five groups. Data were presented as mean ± SD, $n = 3$, ns, no significance, $*p < 0.05$, $**p < 0.01$, $****p < 0.0001$. Color images are available online.

### In vivo *safety evaluation*

Overall, the liver and kidney function indexes of mice (ALT, AST, BUN, and CR) in each group showed an upward trend, indicating that tumor recurrence causes organ damage. In terms of ALT, the ALT of the mice in the multi-GC@PLA group was significantly lower than that in the drug group throughout the observation period (7 days,

$p = 0.0259$; 14 days, $p = 0.0091$; 21 days, $p = 0.0002$), which is almost the same as AST (14 days, $p = 0.0040$; 21 days, $p = 0.0026$). For the renal function test, there was no significant difference in BUN and CR between the multi-GC@PLA group and the drug group at each time point, except that the difference in CR on the 21st day was statistically significant ($p = 0.0116$). On the 21st day, ALT, AST, and CR of the mice
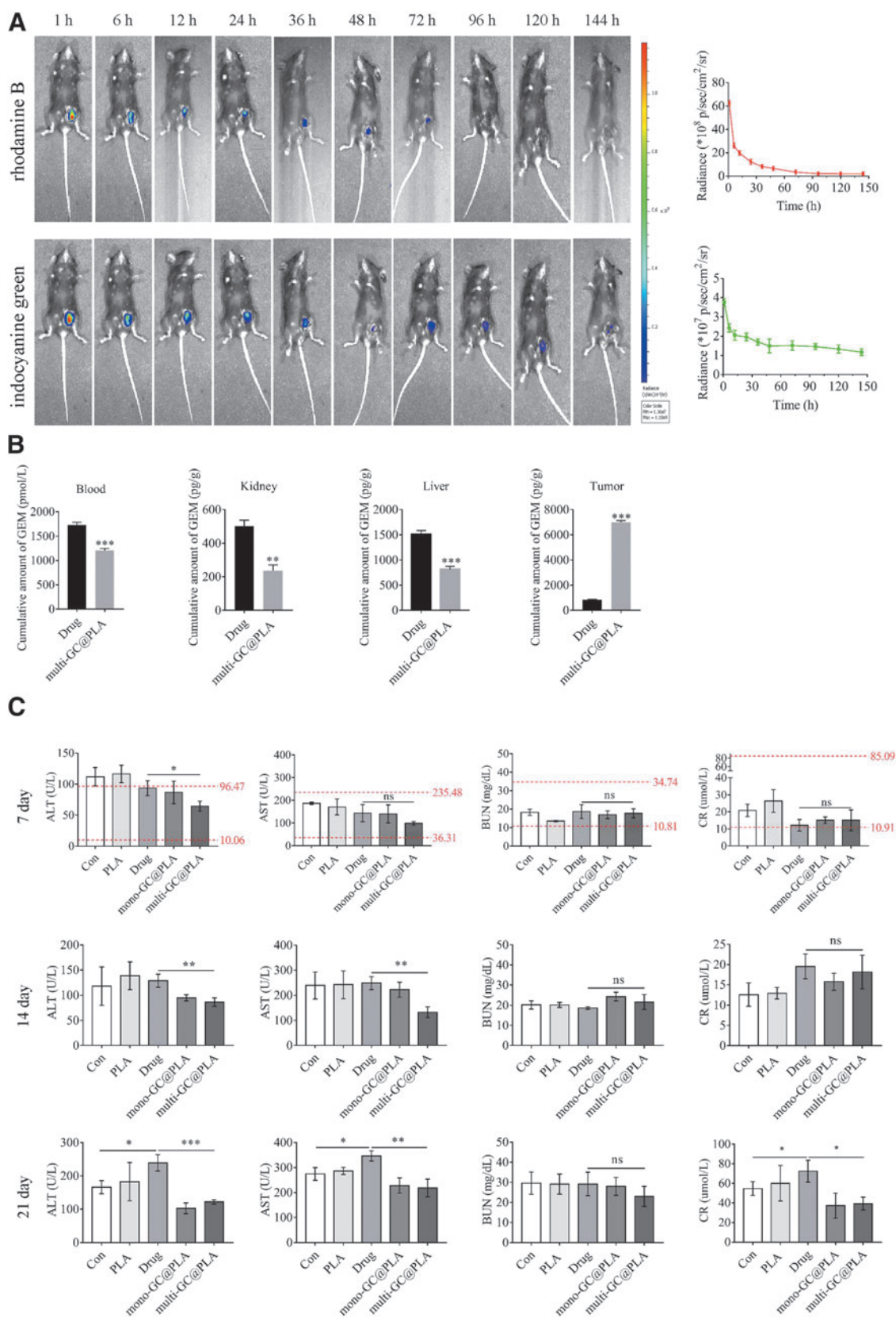
**FIG. 4.** Biodistribution study and safety evaluation. **(A)** Typical fluorescence images of the fiber-covered armpit of healthy C57BL/6 mice after RI@PLA mat implantation and the alteration of fluorescence intensity of rhodamine B and indocyanine *green*. **(B)** Accumulation and distribution of the GEM in the liver, kidney, blood, and tumor tissue. **(C)** Alteration of the AST, the ALT, the BUN, and CR on the 7th, 14th, and 21st day after tumor resection and fiber mats implantation. The normal range was labeled. AST, aspartate aminotransferase; ALT, alanine aminotransferase; CR, creatinine; BUN, blood urea nitrogen. Data were presented as mean ± SD, $n = 3$, ns, no significance, $*p < 0.05$, $**p < 0.01$, $***p < 0.005$. Color images are available online.
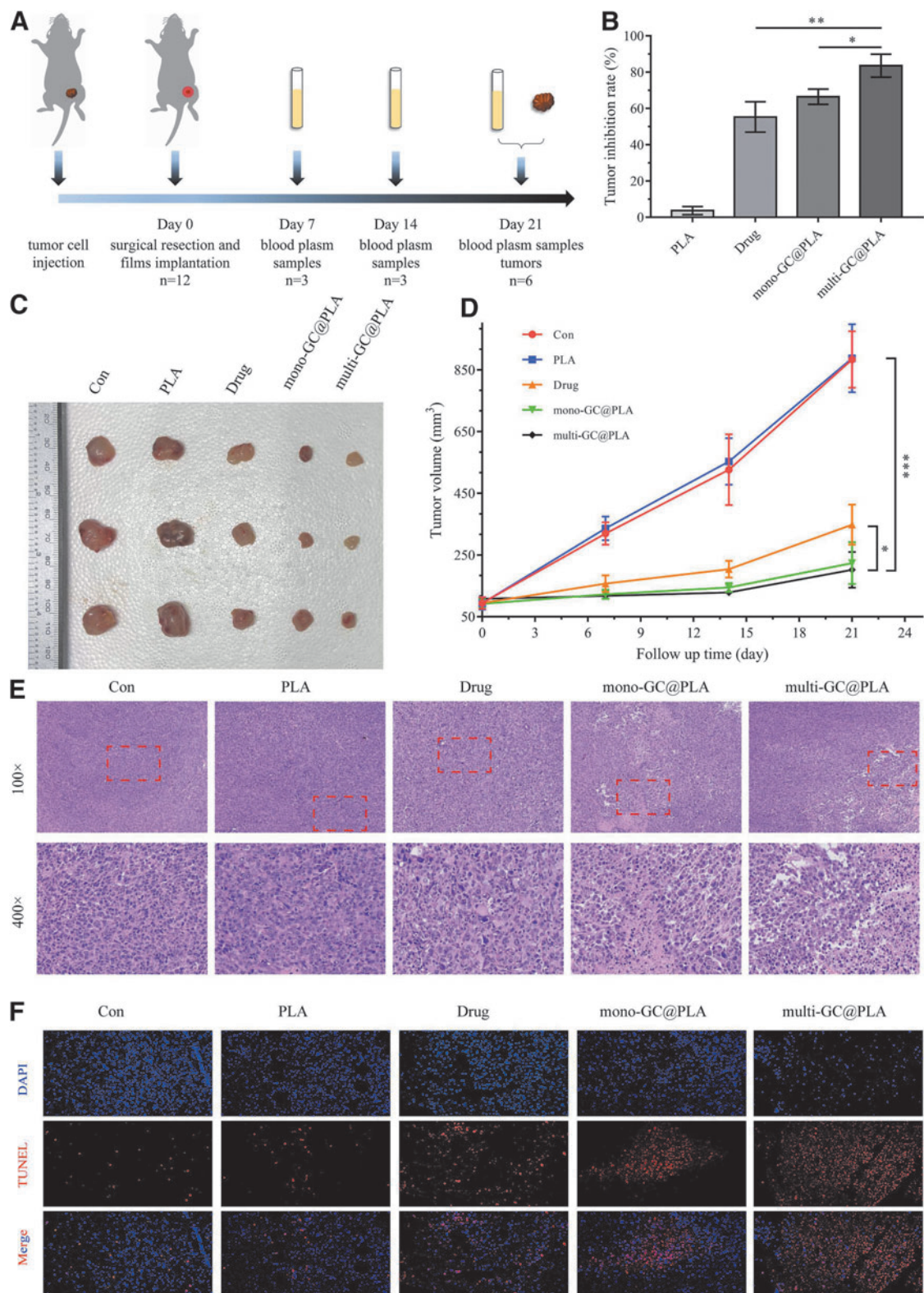
**FIG. 5.** Antitumor activity of drug-loaded nanofilms against the tumor. **(A)** Process of the animal study. **(B)** Tumor inhibition rate. **(C)** Typical images of subcutaneous tumors after drug-loaded nanofilm implantation for 21 days. **(D)** Alteration of the tumor volume. **(E)** Typical images of the H&E staining of subcutaneous tumors. **(F)** Typical images of the TUNEL fluorescence staining of subcutaneous tumors. Data were presented as mean±SD, $n=6$, ns no significance, $*p < 0.05$, $**p < 0.01$, $***p < 0.005$. Color images are available online.

in the drug group were higher than in the Con group ($p = 0.0403$, $p = 0.0380$, $p = 0.0383$) (Fig. 4C).

### In vivo *antitumor efficacy*

The protocol of the animal study is shown in Figure 5A. The tumor inhibition rate in the multi-GC@PLA group was significantly higher than that in the drug group ($83.64 \pm 3.67$ vs. $55.3 \pm 4.83$, $p = 0.0095$), and the mono-GC@PLA group ($83.64 \pm 3.67$ vs. $66.5 \pm 2.43$, $p = 0.0176$) (Fig. 5B). Figure 5C showed the general view of the tumors on the 21st day after the operation. During the observation period (21 days), the residual tumor tissues in each group were growing. The tumor growth of the Con group and the PLA group was fast, and that of the mono-GC@PLA group, the multi-GC@PLA group, and the drug group was slow. On the 21st day after drug-loaded mat implantation, the tumors in the multi-GC@PLA group were significantly smaller compared with the Con group and the drug group ($201.9 \pm 33.43$ vs. $883.5 \pm 53.02\,mm^3$, $p = 0.004$; $201.9 \pm 33.43$ vs. $348.6 \pm 37.56\,mm^3$, $p = 0.0433$) (Fig. 5D).

Apparent necrosis can be observed in the H&E staining of tumor tissue sections of the multi-GC@PLA group, showing poor growth and atypical morphology of tumor cells compared with that of the Con group (Fig. 5E). As shown in Figure 5G, the image of TUNEL fluorescence staining showed that a large number of apoptotic cells existed in the tumor tissues of the multi-GC@PLA group (Fig. 5F). Quantitative analysis revealed that the apoptosis ratio in the multi-GC@PLA group was significantly more prominent than in the Con group and the drug group ($p < 0.0001$; $p = 0.0002$) (Supplementary Fig. S3).

### Discussions

In clinical practice, medicinal mats are widely used as topical, and transdermal delivery systems to achieve anti-inflammatory and analgesic.[19] The application of medicinal mats for antitumors mainly remains in laboratory.[20–22] Localized medicinal patches may be a practical choice for BC with frequent local recurrence. Herein, we utilized sequential electrospinning to fabricate a multilayer mat, in which GEM and CDDP were electrospun individually in distinct layers. Two PLA layers wrapped the G@PLA layer as the inner layer, blocked from the outer layer, the C@PLA layer. By the designing structure, the multilayer mat in our study was capable of sustainedly delivering antitumor agents and prolonging GEM release. Based on the drug-releasing curve, the dissolution equilibrium of the mono-GC@PLA mat was reached at 8 h, whereas the multi-GC@PLA mat was at about 13.8 h, revealing that the multilayer nanofiber mat could prolong the release of GEM compared with the mono-GC@PLA mat.

The results of the *in vitro* experiments preliminarily confirmed the antitumor activity of the multi-GC@PLA mat. The apoptosis of tumor cells can be observed quickly after adding chemotherapy drugs directly into the cell culture system. In contrast, the deadly effect of the drug-loaded mat on tumor cells was delayed. Our results are consistent with the previous researches.[6,16,23] With the degradation of nanofibers, the loaded drugs gradually release and eliminate tumor cells, showing a continuous antitumor feature.

Moreover, antitumor efficacy *in vivo* of the drug-loaded nanofibrous mat was evaluated through a BC positive surgical margin model in the C57BL/6 mice. During the whole observation period, the growth of residual tumors was significantly inhibited, and apparent necrosis could be observed in the tumor tissue. The histological results further proved that a drug-loaded fibrous mat implanted at the tumor site could promote tumor cell apoptosis and thus prevent local recurrence. The antitumor effect of the multi-GC@PLA mats was optimized compared with the mono-GC@PLA mats.

In actual clinical applications, platinum-based drugs are highly cytotoxic, and the primary manifestation is liver and kidney toxicity.[24] Meaningfully, in this study, implanted drug-loaded mat, compared with systemic chemotherapy, scarcely damages liver and kidney function. Chemotherapy drugs were continuously released from the drug-loaded fibrous mat and mainly accumulated *in situ*, without peripheral blood circulation, reducing accumulation in other organs. In the animal fluorescence imaging experiments, it was observed that rhodamine B and indocyanine green, which replaced GEM and CDDP, were mainly concentrated in the implanted site.

The research has some limitations. The drug release *in vivo* could not be fully simulated since lactic acid could be metabolized in the body. Liver injury caused by liver metastasis of tumor cells can contribute to elevated AST and ALT, and protein consumption caused by tumor cells can cause elevated BUN, which may cause errors in experimental measurement. Limited by the sample size and experimental observation period, the results of animal experiments should be treated with caution. However, the results confirmed that the drug-loaded mats could effectively inhibit tumor growth and reduce the toxic side effects. In addition, our study provided a new strategy for co-loading two or more drugs for solid tumor postoperative local chemotherapy or combined with other treatment methods (magnetic therapy and phototherapy) combined treatment.

### Conclusions

In conclusion, a new drug delivery carrier was prepared by sequential electrospinning. The designed mats can achieve two chemotherapeutic drugs (GEM and CDDP) co-loading and time-programmed sustained release, significantly improving our previous study. Through the experiments *in vivo* and *in vitro*, the antitumor effect of the drug-loaded mat was adequately verified. We expect to bring a new strategy of topical chemotherapy for treating solid tumors with positive surgical margins.

### Acknowledgments

### Authors' Contributions

Methodology, investigation, formal analysis, writing—original draft, and writing—review and editing by J.W. Conceptualization, investigation, formal analysis, and writing—original draft by Y.Z. Methodology, investigation, and writing—original draft by Z.W. Investigation and formal analysis by H.C. and X.L. Resources, investigation, and formal analysis by Y.Y. Formal analysis and writing—review and editing by X.R., Y.T., and Z.G. Supervision, project administration, and writing—review and editing by X.Z. and M.W.

## Data Availability

All data generated or analyzed during this study are included in this article and its supplementary material files. Further inquiries can be directed to the corresponding author (Prof. XY. Zeng, miwai@163.com).

## Disclosure Statement

The authors report that there are no competing interests to declare.

## Funding Information

## Supplementary Material

Supplementary Figure S1
Supplementary Figure S2
Supplementary Figure S3

## References

1. Sung H, Ferlay J, Siegel RL, et al. Global Cancer Statistics 2020: GLOBOCAN Estimates of Incidence and Mortality Worldwide for 36 Cancers in 185 Countries. CA Cancer J Clin 2021;71(3):209–249; doi:10.3322/caac.21660

2. Witjes JA, Bruins HM, Cathomas R, et al. European Association of Urology Guidelines on Muscle-invasive and Metastatic Bladder Cancer: Summary of the 2020 Guidelines. Eur Urol 2021;79(1):82–104; doi:10.1016/j.eururo.2020.03.055

3. Picozzi S, Ricci C, Gaeta M, et al. Upper Urinary Tract Recurrence Following Radical Cystectomy for Bladder Cancer: A Meta-Analysis on 13,185 Patients. J Urol 2012;188(6):2046–2054; doi:10.1016/j.juro.2012.08.017

4. Dotan ZA, Kavanagh K, Yossepowitch O, et al. Positive surgical margins in soft tissue following radical cystectomy for bladder cancer and cancer specific survival. J Urol 2007;178(6):2308–2312; doi:10.1016/j.juro.2007.08.023

5. Wolinsky JB, Colson YL, Grinstaff MW. Local drug delivery strategies for cancer treatment: Gels, nanoparticles, polymeric films, rods, and wafers. J Control Release 2012;159(1):14–26; doi:10.1016/j.jconrel.2011.11.031

6. Zhang Z, Liu S, Qi Y, et al. Time-programmed DCA and oxaliplatin release by multilayered nanofiber mats in prevention of local cancer recurrence following surgery. J Controll Release 2016;235:125–133; doi:10.1016/j.jconrel.2016.05.046

7. Chen K, Pan H, Yan Z, et al. A novel alginate/gelatin sponge combined with curcumin-loaded electrospun fibers for postoperative rapid hemostasis and prevention of tumor recurrence. Int J Biol Macromol 2021;182:1339–1350; doi:10.1016/j.ijbiomac.2021.05.074

8. Wang J, Wang G, Shan H, et al. Gradiently degraded electrospun polyester scaffolds with cytostatic for urothelial carcinoma therapy. Biomater Sci 2019;7(3):963–974; doi:10.1039/c8bm01317a

9. Liu M, Zhang Y, Sun S, et al. Recent advances in electrospun for drug delivery purpose. J Drug Target 2019;27(3):270–282; doi:10.1080/1061186X.2018.1481413

10. Polakova L, Sirc J, Hobzova R, et al. Electrospun nanofibers for local anticancer therapy: Review of in vivo activity. Int J Pharm 2019;558:268–283; doi:10.1016/j.ijpharm.2018.12.059

11. Xia Q, Zhang N, Li J, et al. Dual-functional esophageal stent coating composed of paclitaxel-loaded electrospun membrane and protective film. J Biomed Nanotechnol 2019;15(10):2108–2120; doi:10.1166/jbn.2019.2838

12. Lian H, Meng Z. Melt electrospinning of daunorubicin hydrochloride-loaded poly (epsilon-caprolactone) fibrous membrane for tumor therapy. Bioact Mater 2017;2(2):96–100; doi:10.1016/j.bioactmat.2017.03.003

13. Zhang J, Wang X, Liu T, et al. Antitumor activity of electrospun polylactide nanofibers loaded with 5-fluorouracil and oxaliplatin against colorectal cancer. Drug Deliv 2016;23(3):794–800; doi:10.3109/10717544.2014.916768

14. Wei J, Luo X, Chen M, et al. Spatial distribution and antitumor activities after intratumoral injection of fragmented fibers with loaded hydroxycamptothecin. Acta Biomater 2015;23:189–200; doi:10.1016/j.actbio.2015.05.020

15. Flaig TW, Spiess PE, Agarwal N, et al. Bladder Cancer, Version 3.2020, NCCN Clinical Practice Guidelines in Oncology. J Natl Compr Canc Netw 2020;18(3):329–354; doi:10.6004/jnccn.2020.0011

16. Zhu Y, Liu S, Feng C, et al. The delivery materials with chemotherapy drugs for treatment of the positive margin in solid tumors. Tissue Eng Part A 2021;27(9–10):536–548; doi:10.1089/ten.TEA.2020.0076

17. Pacardo DB, Ligler FS, Gu Z. Programmable nanomedicine: Synergistic and sequential drug delivery systems. Nanoscale 2015;7(8):3381–3391; doi:10.1039/c4nr07677j

18. Falde EJ, Freedman JD, Herrera VL, et al. Layered superhydrophobic meshes for controlled drug release. J Control Release 2015;214:23–29; doi:10.1016/j.jconrel.2015.06.042

19. Pastore MN, Kalia YN, Horstmann M, et al. Transdermal patches: History, development and pharmacology. Br J Pharmacol 2015;172(9):2179–2209; doi:10.1111/bph.13059

20. Jun E, Kim SC, Lee CM, et al. Synergistic effect of a drug loaded electrospun patch and systemic chemotherapy in pancreatic cancer xenograft. Sci Rep 2017;7(1):12381; doi:10.1038/s41598-017-12670-3

21. Ye Y, Wang C, Zhang X, et al. A melanin-mediated cancer immunotherapy patch. Sci Immunol 2017;2(17):eaan5692; doi:10.1126/sciimmunol.aan5692

22. Han X, Li H, Zhou D, et al. Local and targeted delivery of immune checkpoint blockade therapeutics. Acc Chem Res 2020;53(11):2521–2533; doi:10.1021/acs.accounts.0c00339

23. Ding Q, Li Z, Yang Y, et al. Preparation and therapeutic application of docetaxel-loaded poly(D,L-lactide) nanofibers in preventing breast cancer recurrence. Drug Deliv 2016;23(8):2677–2685; doi:10.3109/10717544.2015.1048490

24. Prsa P, Karademir B, Bicim G, et al. The potential use of natural products to negate hepatic, renal and neuronal toxicity induced by cancer therapeutics. Biochem Pharmacol 2020;173; doi:10.1016/j.bcp.2019.06.007

Address correspondence to:
*Xiaoyong Zeng, MD, PhD*
*Department of Urology*
*Tongji Hospital*
*Tongji Medical College*
*Huazhong University of Science and Technology*
*No.1095 Jiefang Avenue*
*Wuhan 430030*
*China*

*E-mail:* miwai@163.com